Electronic Supplementary Information

Optimal Geometrical Design of Inertial Vibration DC Piezoelectric Nanogenerators Based on Obliquely Aligned InN Nanowire Arrays

Nai-Jen Ku,[a] Guocheng Liu,[b] Chao-Hung Wang,[a] Kapil Gupta,[a] Wei-Shun Liao,[a] Dayan Ban[b] and Chuan-Pu Liu*[a]

[a]Department of Materials Science and Engineering, National Cheng Kung University, Tainan 70101, Taiwan
[b]Department of Electrical and Computer Engineering, University of Waterloo, Waterloo, ON N2L 3G1, Canada

E-mail: cpliu@mail.ncku.edu.tw

The anticipated increasing use of major natural energy resources, which will become extremely scarce, in the coming decades have sparked significant world-wide efforts toward the search for the cost effective renewable and green energy resources to meet future global energy demands. In this regard, advances in self-powered nanotechnology allowing for the design of efficient energy harvesting offers an enormous potential for the creation of sustainable systems utilizing incessantly natural ambient energy resources. Mechanical stress applied to piezotronic materials distorts internal dipole moments, generating electrical potentials in direct proportion to the applied force. Over the years, many kinds of NGs have been demonstrated to make effective use of the mechanical resources with variable frequencies and amplitudes in the environment. With this motivation, over the past few years the techniques of energy harvesting from piezotronic nanomaterials have emerged to reclaim the ambient vibration energy and turn it into electrical power. The NGs based on obliquely aligned InN NW arrays have shown potential applications not

only as an energy harvesting device capable of scavenging energy from mechanical vibrations, but also as a sensitive force sensor which can monitor the behavior of the human heart through the small physical motion of the sphygmus. This supporting information provides detailed information on the numerical calculations of piezopotential distribution in an oblique InN NW, the characteristics of the strain sensor, and the NW structural damping analysis of the output voltage of the NGs.

1. Piezopotential distribution in an oblique InN NW

The bending curvature of the oblique NWs is proportional to the force applied to it. Since a positive piezopotential at the stretched side and a negative piezopotential at the compressed side of a NW are generated, the piezopotential gradient across the NW is proportional to the applied force. The piezopotential generated, is responsible for the output electricity. While the piezopotential has been demonstrated to be related to the aspect ratio of a NW rather than its dimensionality, we show that the piezopotential is also directly related to the tilt angle of an oblique NW relative to the substrate, for a given aspect ratio.

To understand the piezopotential distribution in an oblique InN NW, the Lippmann theory was used in numerical calculations for piezopotential by finite element simulations.[1,2] The piezopotential distribution in a bent oblique InN NW was calculated under a force of 80 nN along different exerted directions. Although the magnitude of the piezopotential is influenced by the carrier concentration, a clear physical picture for quasi-quantitative understanding can still be gained by numerical calculations without considering the charge carrier density.[1] The material constants of InN adopted in the calculations are: density ρ = 6810 Kg/m^3, lattice constants a = 3.536 Å, c = 5.709 Å; elastic constants C_{11} = 223 GPa, C_{12} = 115 GPa, C_{13} = 92 GPa, C_{33} = 224 GPa, C_{44} = 48 GPa; piezoelectric constants $e_{15} = e_{31} = -0.57$ C/m^2, e_{33} = 0.97 C/m^2, and dielectric constants $\varepsilon_{11} = \varepsilon_{12}$ = 13.1, ε_{33} = 14.4.[2] The diameter and the length of the InN NWs are kept constant at 50 nm and 1 μm, respectively, while the c-axis of the NW remains perpendicular to the substrate throughout the calculations. The influence of varying the tilt angle of the InN NW on piezopotential distribution is systematically investigated.

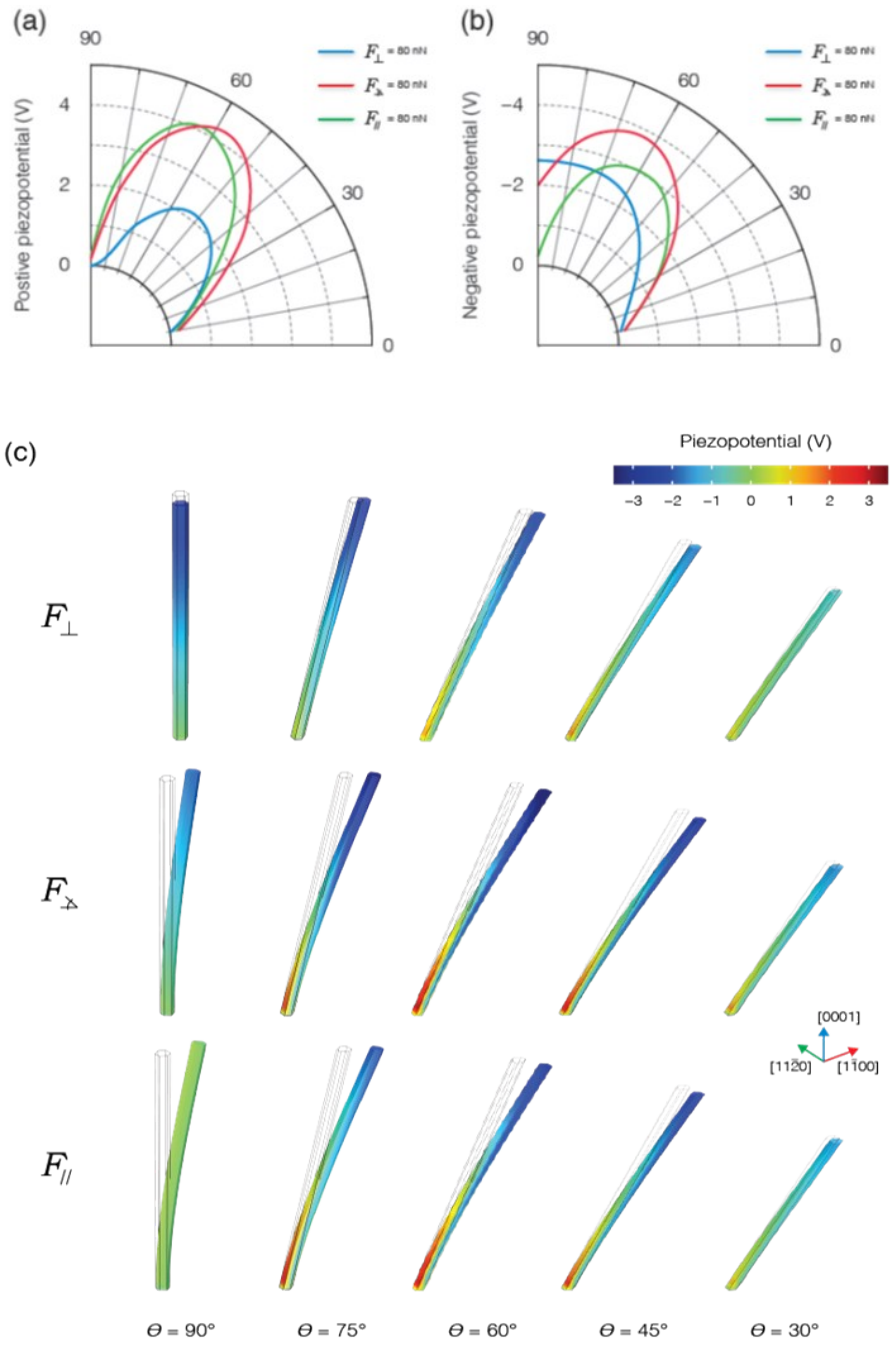

Figure S1: Angular distribution of (a) positive and (b) negative piezopotential of an oblique InN NW as a function of tilt angle. (c) Calculated piezopotential distribution within an InN NW in the tilt angles of 90°, 75°, 60°, 45°, and 30° with length = 1 μm and diameter = 50 nm. The exerted force sets to 80 nN along the $[000\bar{1}]$, $[1\bar{1}00]$, and $[1\bar{1}0\bar{1}]$ directions designated as $F_\perp$, $F_{//}$, and $F_\nearrow$, respectively.

The InN NWs shown in Figure 1(b) in the manuscript grow obliquely on the substrate and subtend an angle of $\theta = 58°$ relative to the substrate. Therefore, we assume that an oblique NW is fixed at one end (bottom side) and the other end is pushed by a point force, analogous to the action of the top pyramidal electrode, with the magnitude of 80 nN along the $[000\bar{1}]$, $[1\bar{1}00]$, and $[1\bar{1}0\bar{1}]$ directions designated as $F_{\perp}$, $F_{\parallel}$, and $F_{\measuredangle}$, respectively. The stretched and compressed sides of the NW correspond to positive and negative piezopotentials, respectively. When the pyramidal electrode scans across the top of the NW during the course of push-down and touches the compressed side of the NW, the negative piezopotential sets the Schottky diode to forward bias, thus the free electrons can flow across the interface, resulting in a transient current in the external load. Therefore, the magnitude of the negative piezopotential at the top of the NW would govern the measured output voltage via the external load. Both maximum positive and negative piezopotentials are plotted as a function of the tilt angles of the NW, as shown in Figure S1(a−b). The plots of numerical calculation results shown in Figure S1(c) represent the piezopotential distributions inside the NW upon bending by the force, where the tilt angles of NWs varied from 90° to 30°.

Based on the results, it is found that the magnitude and distribution of the piezopotential in a bent NW would strongly depend on the growth direction of the NW. The positive and negative piezopotentials for the vertical NW ($\theta = 90°$) under the lateral deflection force $F_{\parallel}$, as applied in the major DC-NG operation mode, is calculated to be 0.268 V and − 0.267 V, respectively. These values are consistent with the numerical results reported by Huang et al.[2] Both the positive and negative piezopotentials will increase for a bent oblique InN NW and the maxima occur for a NW with the tilt angle of $\theta = 60°$, which are 3.021 V and −3.079 V, respectively, almost 11.3 times larger than those of a vertical NW with the same diameter, length, and applied force.

When a force is applied along the $[000\bar{1}]$ direction as a normal force $F_{\perp}$ in the AC-NG operation mode, this force can generate the maximum negative piezopotential of −2.620 V for the vertical NW (θ = 90°) as compared to the other two types of forces. However, the maximum positive piezopotential of 1.677 V occurs for an oblique NW with the tilt angle of θ = 50°. Thereby, the maximum piezopotential difference (ΔV_{piezo}) generated by a normal compressive force to an InN NW occurs for an oblique NW with the tilt angle of about θ = 60°, reaching 3.783 V.

The global maximum occurs for the force exerted along the $[1\bar{1}0\bar{1}]$ direction ($F_{\measuredangle}$) on an oblique NW with the tilt angle of θ = 60°, where the contributions come from the force for both bending and pushing along the polar direction, leading to the significant enhancement in both positive and negative piezopotentials to 4.267 and −3.813 V at the stretched and compressed side of the NW, respectively. Our results indicate that the tilt angle of the NW around θ = 60° is the best geometry for the highest piezopotential to be applied in DC/AC nanogenerators or nanopiezotronics.

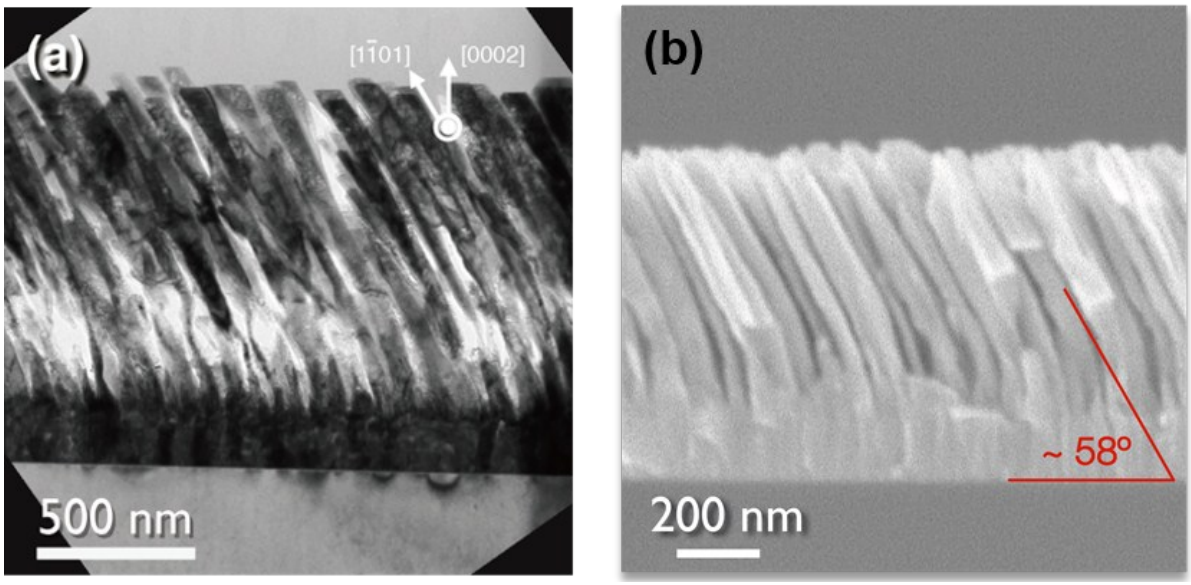

Figure S2: Cross-sectional (a) TEM and (b) SEM images of obliquely aligned InN nanowire arrays, grown on Al:ZnO nano-pillars.

S2. The change of SBH with strain in the NG

The Schottky junctions form at the interfaces between the Pt-coated Si-pyramidal electrode and InN NWs and can be described by the thermionic-emission-diffusion (TED) model. The TED theory attempts to explain the *I-V* behavior of Schottky junction. Assuming that the SBH, ϕ_s, is larger than kT, the current density is given as: [3-5]

$$J_{TED} = A^{**}\ T^2\ exp\left(-\frac{\phi_s}{kT}\right)exp\left(\frac{q\phi_f}{kT}\right)$$

$$\phi_f = \sqrt{\frac{qE_m}{4\pi\varepsilon_s}},\quad E_m = \sqrt{\frac{2qN_D^+}{\varepsilon_s}\left(V + V_{bi} - \frac{kT}{q}\right)} \tag{1S}$$

where A^{**} is the effective Richardson constant, q is the electron charge, k is the Boltzmann constant, ϕ_f is the image force correction, N_D^+ is the donor concentration, V is the applied voltage, V_{bi} is the built-in potential at the barrier, and ε_s is the permittivity of InN.

According to the theory of piezotronics, the change in the effective SBH induced by the piezopotential is linearly dependent on the density of polarization charges, ρ_{piezo}:[6]

$$\Delta\phi_s = \phi_s - \phi_{s0} = -\frac{q^2\rho_{piezo}W_{piezo}^2}{2\varepsilon_s} \tag{2S}$$

$$\rho_{piezo} = \frac{F}{IY}[2(1+\nu)e_{15} + 2\nu e_{31} - e_{33}]r \tag{3S}$$

where W_{piezo} is the depletion layer width of the piezocharges, F is the applied force, I is the moment of inertia of the InN NW, Y is the Young's modulus of the InN NW, ν is the Poisson ratio, e_{ij} is the piezoelectric coefficient, and r is the radius of the InN NW. From the equations (1S-3S), the change in the natural logarithm of the current density could be inferred from the force/strain, as shown in Figure 6(b).

S3. Output voltage oscillation and damping effect

Figure S3(a−b) shows the V_{oc} waveforms of a single NG and two NGs connected in series excited at 5 Hz, respectively. Their corresponding Fourier spectra are shown in Figure S3(c−d) covering the entire frequency range. It is interesting to note that there is no dominant peak at 5 Hz frequency (excitation frequency of the shaker) in both J_{sc} and V_{oc}, exhibiting unsynchronized movements of InN NWs and top pyramidal electrode. Instead, the dominant frequencies are located at 0.1 ~ 0.3 and 1.9 Hz for V_{oc}. In contrast to the single peak at ~ 1.9 Hz, the multiple peaks with a regular interval at low frequencies are ascribed to the long-period oscillations in Figure 3(b). The long-period multimode oscillations in V_{oc} at 0.1 ~ 0.3 Hz are converted to approximately 37 sinusoids, corresponding to the most prominent oscillations of ~ 1.9 Hz, revealing a large number of additional significant frequencies. The region between 0.1 and 0.3 Hz shows a clear pattern of roughly equally spaced peaks, interpreted as high-order consecutive overtones. The comb-like structure expected for high-order overtones is clearly visible with the frequency separation Δv, indicating the frequency separation between consecutive overtones. For such oscillations, the observed comb-like frequency structure is the result of the damped oscillation between the oblique NWs and the top pyramidal electrode. The strikingly broadened structures observed only at low frequencies suggest to be due to damped and re-excited oscillations or very close unresolved frequencies of coherent oscillations for the NW and the electrode. For the two serial connected NGs shown in Figure S3(d), the high-frequency peak shifts from 1.9 Hz to ~ 0.9 Hz, which is about half of that for a single NG.

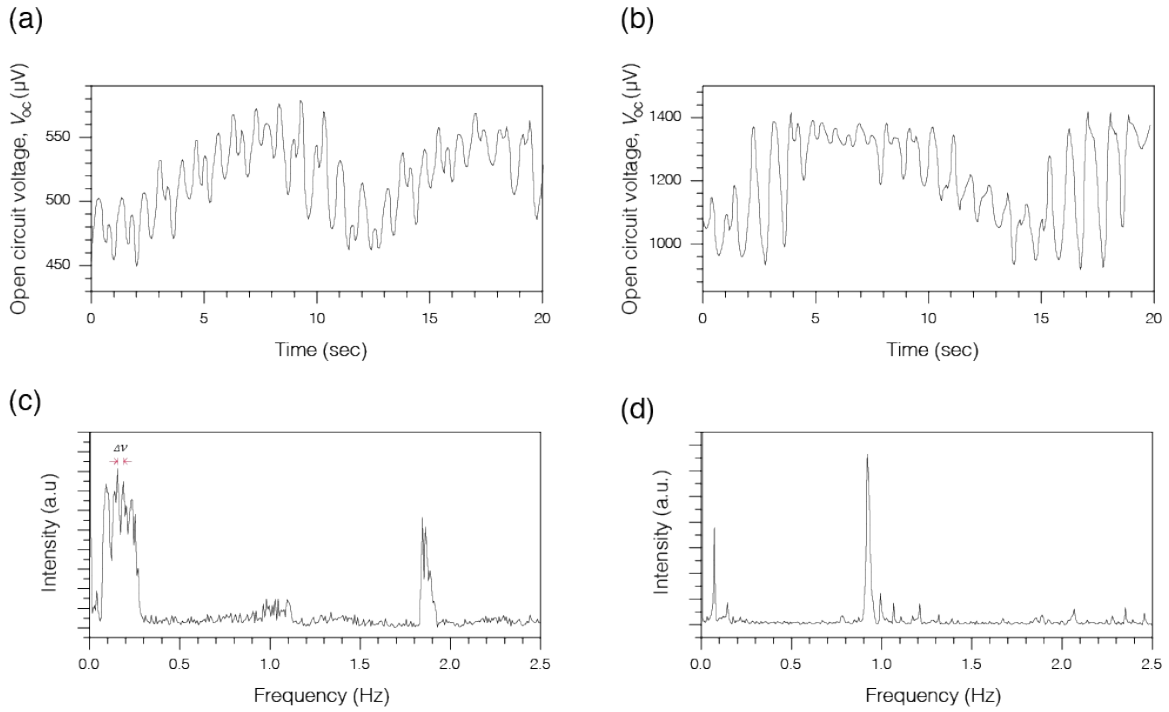

Figure S3: Output voltage (V_{oc}) waveforms of (a) a single NG and (b) two NGs connected in series. (c,d) are the corresponding Fourier spectra of (a,b), respectively.

Figure S4(a−b) shows the J_{sc} waveforms of a single NG and two NGs connected in parallel, respectively, with their corresponding Fourier spectra shown in Figure S4(c−d). Comparing to the V_{oc} signals, the variation of the J_{sc} waveforms is much flattened. Because the voltages created by all of the NWs are in parallel for the NG, each individual NW could determine the magnitude of the output voltage. Therefore, V_{oc} appears relatively sensitive to the unsynchronized oscillation between the NWs and pyramidal electrode. On the other hand, the output current is a sum of the current produced by all the active NWs. Therefore, the J_{sc} signals are more stable and continuous.[8] The dominant Fourier peak occur only at 1.9 Hz without any comb-like features in the low frequency region, unlike V_{oc}. For the parallel connection of two NGs, the peak frequency also shifts from 1.9 Hz to ~ 0.9 Hz, which is consistent with the V_{oc} signals.

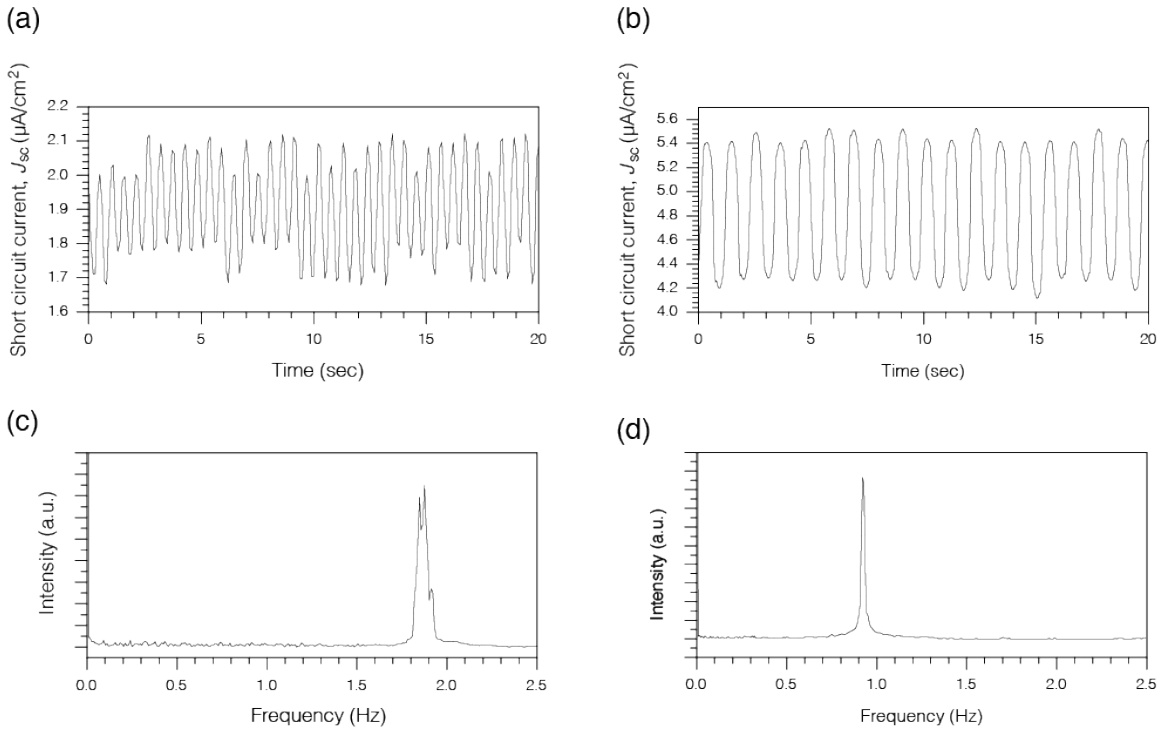

Figure S4: Output current density (J_{sc}) waveforms of (a) a single NG and (b) two NGs connected in parallel. (c,d) are the corresponding Fourier spectra of (a,b), respectively.

SUPPORTING REFERENCES

(1) Gao, Y.; Wang, Z. L., *Nano Lett.* **2009,** 9 (3), 1103.

(2) Huang, C. T.; Song, J.; Tsai, C. M.; Lee, W. F.; Lien, D. H.; Gao, Z.; Hao, Y.; Chen, L. J.; Wang, Z. L., *Adv. Mater.* **2010,** 22 (36), 4008.

(3) Zhou, J.; Fei, P.; Gu, Y.; Mai, W.; Gao, Y.; Yang, R.; Bao, G.; Wang, Z. L., *Nano Lett.* **2008,** 8 (11), 3973.

(4) Zhou, J.; Gu, Y.; Fei, P.; Mai, W.; Gao, Y.; Yang, R.; Bao, G.; Wang, Z. L., *Nano Lett.* **2008,** 8 (9), 3035.

(5) Sze, S. M.; Ng, K. K., *Physics of Semiconductor Devices*. 3rd ed.; Wiley-Interscience: Hoboken, New York, 2006.

(6) Zhang, Y.; Liu, Y.; Wang, Z. L., *Adv. Mater.* **2011,** 23 (27), 3004.

(7) Zhou, Y. S.; Hinchet, R.; Yang, Y.; Ardila, G.; Songmuang, R.; Zhang, F.; Zhang, Y.; Han, W.; Pradel, K.; Montes, L.; Mouis, M.; Wang, Z. L., *Adv. Mater.* **2013,** 25 (6), 883.

(8) Wang, X.; Song, J.; Liu, J.; Wang, Z. L., *Science* **2007,** 316 (5821), 102.

(9) Xu, S.; Qin, Y.; Xu, C.; Wei, Y. G.; Yang, R. S.; Wang, Z. L., *Nat. Nanotechnol.* **2010,** 5 (5), 366.